An automated and compartmented fluidic reactor device for multi-step sample-to-answer processes using magnetic particles

J. Hübner, R. Heinzler, C. Arlt, S. Hohmann, G. Brenner-Weiß and M. Franzreb

Karlsruhe Institute of Technology (KIT), Institute of Functional Interfaces (IFG), Eggenstein-Leopoldshafen, Germany
E-mail: jonas.huebner@kit.edu

Supplement

2 Layout drawing of the magnetic field module

Detailed layout drawing of the MFM for magnetic particle processing. A compact baseplate I positions a capillary holder II that centers a reaction capillary III between two coils IV. The coils generate an electromagnetic field for particle resuspension that may be increased inserting mild steel cylinders V. For automated separation, beneath the capillary a permanent magnet array VI is mounted on a lever VII that is moved by a standard servo VIII.

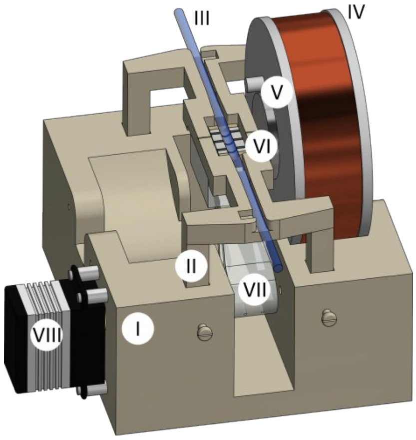

Fig. **1** Detailed layout drawing of the MFM.

3 Calculation of the magnetic field inside the Helmholtz coil

The method, adapted after Huber and Urban[32] and Kirschvink[33], uses cylindrical coordinates for a point P in space (r, z) of a circular coil system with a given radius a in the $r - \theta$ plane, mounted in a distance b with the center at the origin. Like that, the magnetic flux density at an electrical permeability μ ($T \cdot m \cdot A^{-1}$) wired with N windings and operated by a current I (in A) is not expressible in terms of analytical functions but can be expressed as shown for B_r and B_z in eqn. 5 and 6. Herein, K and E (eqn. 7) are elliptic integrals of the first and second kind. The functions of K and E, with $k/\tilde{k}$ as defined in eqn. 8, have polynomial approximations accurate in the range of 10^{-8} that are evaluable numerically.

Subsequently, the magnetic field can be computed leading to the radial and axial vector components B_r and B_z (T). $B_{\square}$ is, due to symmetry in the cylindrical coordinate system, zero.

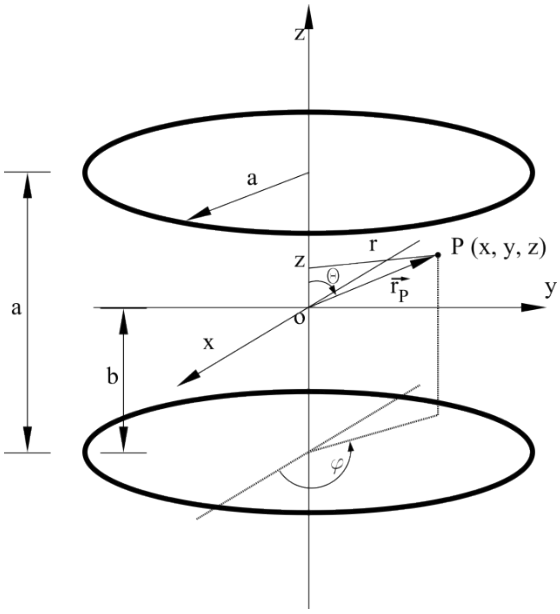

Fig. 2 Geometric representation for the calculation of the magnetic flux at any point P in the median plane of a Helmholtz coil arrangement.

$$B_r = \frac{\mu\, I\, N 1}{2\pi\ r}\left\{\frac{(z+b)}{\sqrt{(a+r)^2+(z+b)^2}}\left[-K(k)+\frac{a^2+r^2+(z+b)^2}{(a-r)^2+(z+b)^2}E(\right.\right. \tag{5}$$

$$B_z = \frac{\mu\, I\, N}{2\pi}\left\{\frac{(z+b)}{\sqrt{(a-r)^2-(z+b)^2}}\left[-K(k)+\frac{a^2+r^2+(z+b)^2}{(a-r)^2+(z+b)^2}E(k \right.\right. \tag{6}$$

$$K(k) = \int_0^{\frac{\pi}{2}} \frac{d\varphi}{\sqrt{1-k^2 sin^2\varphi}} \qquad E(k) = \int_0^{\frac{\pi}{2}} \sqrt{1-k^2 sin^2\varphi}\, d\varphi \tag{7}$$

$$k = \sqrt{\frac{4ar}{(a+r)^2+(z+b)^2}} \qquad k = \sqrt{\frac{4ar}{(a+r)^2+(z-b)^2}} \tag{8}$$

4 Electromagnetic field characterization

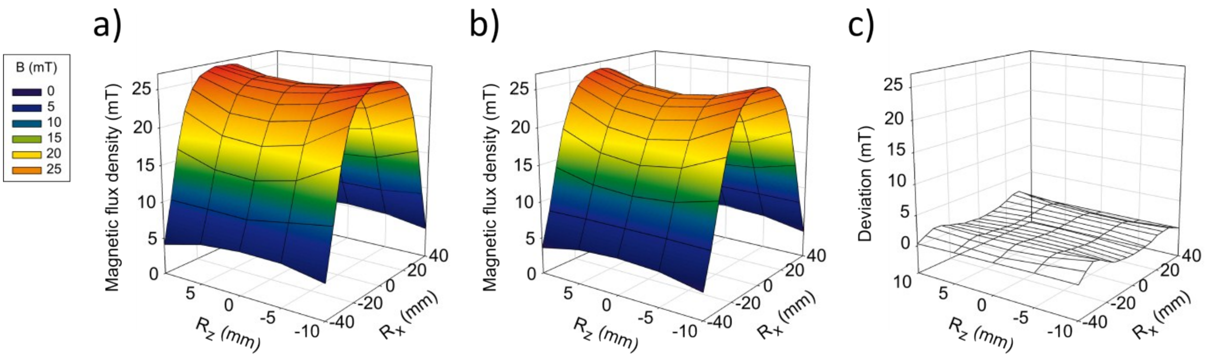

Fig. **3** a**)** Contour plot of the magnetic field uniformity of the MFM gained from transversal hall probe measurements. **b)** Results of the numeric computing simulation of the developed system. **c)** Deviation between measurement and calculation results.

5 Evaluation of compartment sizes

Analysis of the set of imaged aqueous compartments was performed using the imageJ distribution FIJI. A tailor-made macro tool set was build using FIJI implemented functions to automatically process the exported images as follows: First, a global scale was set up using the outer diameter of the capillary as reference structure. Images were then cropped to the area of interest, converted to 8-bit grayscale and the FIJI implemented threshold *minimum* was applied to define the dyed compartments as the image *foreground*. Subsequently *analyze particles* was executed filtering all objects on the foreground according to size and circularity whereas in all operations all objects ≥ 0.05 µm^2 where taken into account – smaller objects were excluded. Additionally, shapes that are touching the edge of the cropped image were excluded. All objects that fulfill these criteria were defined as compartments and their areas were calculated based on the global scaling and listed in a tabulated data sheet.

The volume of the defined compartments was calculated based on the cross-sectional area data for each reaction compartment. Since there is no satisfactory method to calculate the volume of the rod shaped compartments (Fig. 4a) directly, previously the cross-sectional areas of the two object endings were measured in a separate experiment and subsequently deducted from the cross-sectional area of each compartment (Fig. 4b). As the inner diameter of the capillary is known, the volume of the cylinder, as shown in Fig. 4c, could then be calculated. In the next step, two times the volume of a standardized half ellipsoid compound was added to the volume of the core cylinder (Fig. 4d). As the meniscus of a phase boundary in a certain two phase system with constant surface tension is constant, the two volumes for the ellipsoid compartment endings were, as mentioned for process step b), determined separately in preliminary experiments (data not shown) and used for all calculations. Finally, as visualized in Fig. 4e, the volume of the entire geometrical entity was calculated by summarizing the volumes of the core cylinder structure and the two half ellipsoid endings.

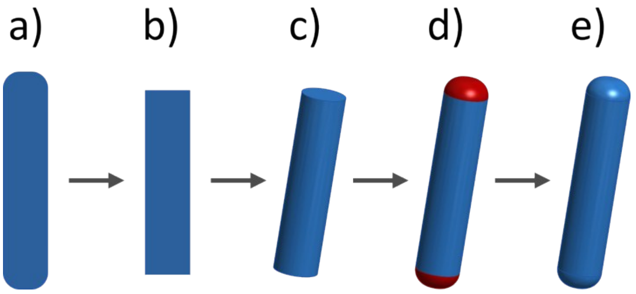

Fig. 4 Schematic work flow of the compartment volume calculation process. Based on the 2D compartment cross-sectional area given out by the FIJI macro set **a)**, at first the area representing the two object endings is deducted **b)** to calculate the volume of the received cylinder **c)**. Separately determined volumes of two standardized half ellipsoid compounds are then added to the volume of the cylindrical core structure **d)** resulting in the calculated volume of the entire compartment **e)**.

6 ESEM imaging of device processed particles

As the ESEM images indicate, no effect on the magnetic particle surface morphology could be detected. This might give proof, that the electromagnetic field driven particle rotation neither damaged the particles nor influenced their surface and make this process suitable as a sustainable method for magnetic particle resuspension.

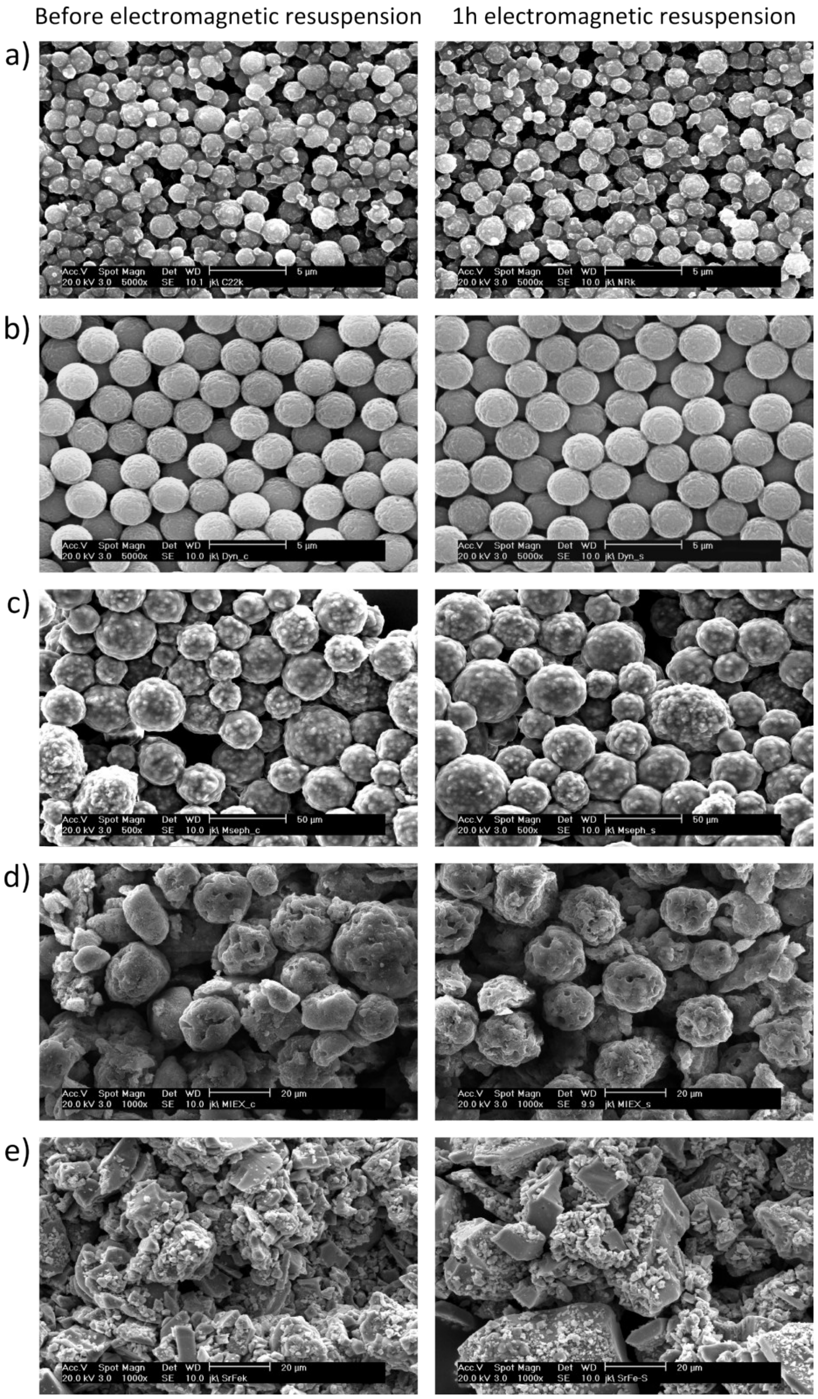

Fig. 5 ESEM imaging of the tested particles collection before (panels on the left) and after (panels on the right) 1 h electromagnetically resuspension. **a)** M-PVA, **b)** Dynabeads, **c)** Mag Sepharose, **d)** MIEX and **e)** Strontium ferrite.

7 Particle size distributions before and after reactor device processing

Particle magnetization based on the electrical as well as permanent magnetic field did not seem to change the particle size distribution. M-PVA, Dynabeads Mag Sepharose, and MIEX did not show a changed mean surface weighted particle diameter. The result slightly differed for strontium ferrite particles. Due to the high residual magnetization of the particle types, the mean surface weighted particle diameter of strontium ferrite increased from 22.5 ±14.0 to 31.2 ±16.8 µm (Table 4). Also, as visualized in the size distribution plots, the measured size distribution changed and more big sized agglomerates occurred. Besides that, the ESEM images of the strontium ferrite particles recorded after the magnetic treatment showed smallest flakes being attached to bigger particles.

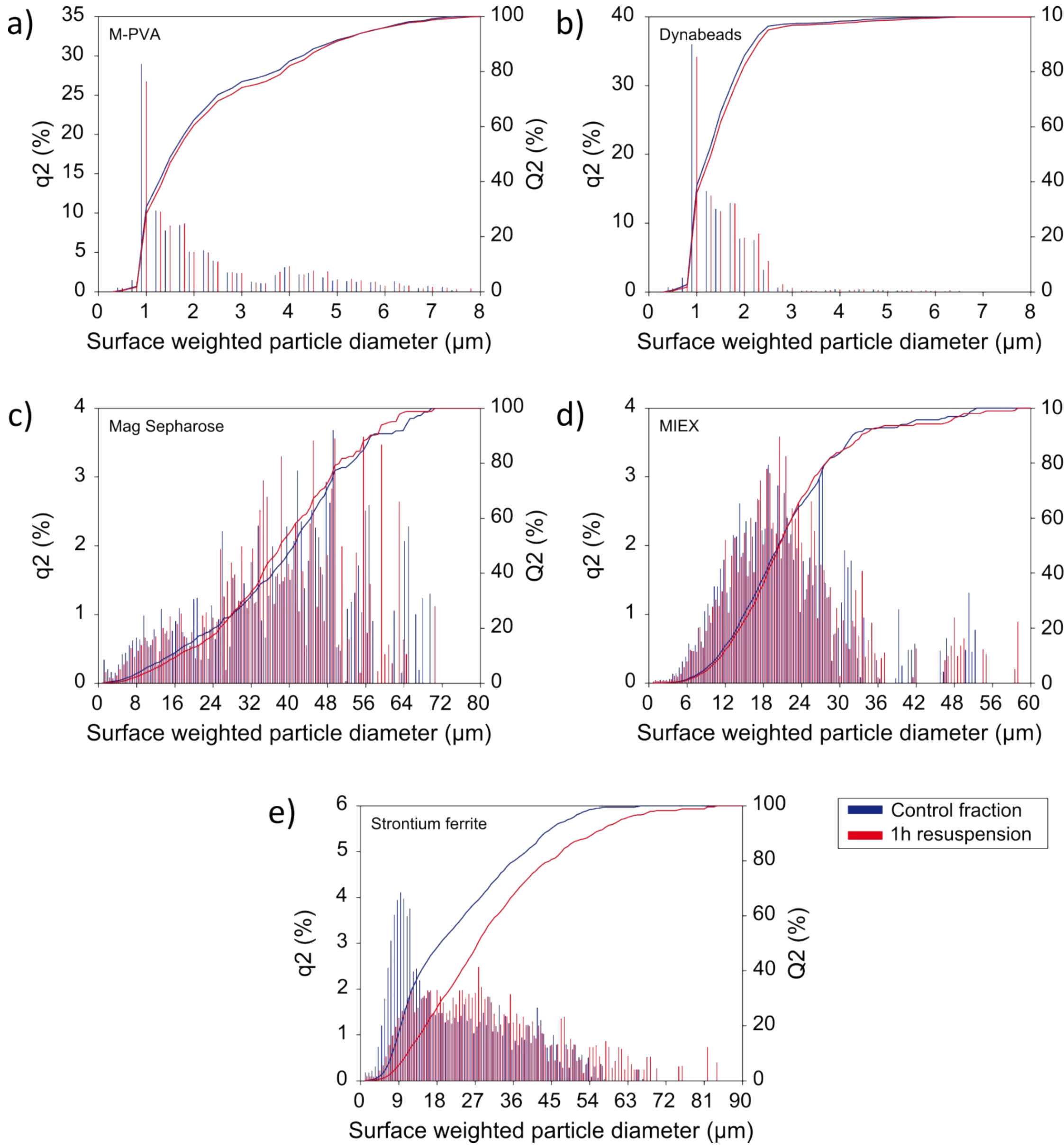

Fig. 6 Size distribution comparison of the surface weighted particle diameter of the tested particles collection before and after 1 h electromagnetically resuspension. **a)** M-PVA, **b)** Dynabeads, **c)** Mag Sepharose, **d)** MIEX and **e)** Strontium ferrite.